

Contents lists available at ScienceDirect

Petroleum Science

journal homepage: www.keaipublishing.com/en/journals/petroleum-science



Original Paper

Fluid discrimination incorporating viscoelasticity and frequencydependent amplitude variation with offsets inversion



Zhao-Yun Zong*, Yan-Wen Feng, Xing-Yao Yin, Kun Li, Guang-Zhi Zhang

Department of Geophysics, School of Geosciences, China University of Petroleum (East China), Qingdao, Shandong, 266580, China

ARTICLE INFO

Article history: Received 29 July 2020 Accepted 5 January 2021 Available online 12 July 2021

Edited by Jie Hao

Keywords:
Frequency-dependent
Viscoelasticity
Solid-liquid decoupling fluid factor
FAVO inversion
Fluid discrimination

ABSTRACT

Frequency-dependent amplitude versus offset (FAVO) inversion is a popular method to estimate the frequency-dependent elastic parameters by using amplitude and frequency information of pre-stack seismic data to guide fluid identification. Current frequency-dependent AVO inversion methods are mainly based on elastic theory without the consideration of the viscoelasticity of oil/gas. A fluid discrimination approach is proposed in this study by incorporating the viscoelasticity and relevant FAVO inversion. Based on viscoelastic and rock physics theories, a frequency-dependent viscoelastic solid-liquid decoupling fluid factor is initially constructed, and its sensitivity in fluid discrimination is compared with other conventional fluid factors. Furthermore, a novel reflectivity equation is derived in terms of the viscoelastic solid-liquid decoupling fluid factor. Due to the introduction of viscoelastic theory, the proposed reflectivity is related to frequency, which is more widely applicable than the traditional elastic reflectivity equation directly derived from the elastic reflectivity equation on frequency. Finally, a pragmatic frequency-dependent inversion method is introduced to verify the feasibility of the equation for frequency-dependent viscoelastic solid-liquid decoupling fluid factor prediction. Synthetic and field data examples demonstrate the feasibility and stability of the proposed approach in fluid discrimination.

© 2021 The Authors. Publishing services by Elsevier B.V. on behalf of KeAi Communications Co. Ltd. This is an open access article under the CC BY-NC-ND license (http://creativecommons.org/licenses/by-nc-nd/4.0/).

1. Introduction

Fluid discrimination with seismic data helps to predict the distribution of the oil/gas reservoirs by analyzing the changes of seismic wave velocity, amplitude, frequency and waveform etc. In recent years, a variety of fluid anomaly identification methods based on seismic data have been proposed. From the perspective of seismic information, it can be divided into the method of fluid identification using amplitude information, frequency information, phase information or waveform information (Backus and Chen, 1975; Tatham, 1982; Mazzotti, 1991; Chen et al., 2008; Ren et al., 2009; Ahmed, 2012; Zhu and McMechan, 2012; Yao and Wu, 2017; Yao et al., 2020); from the realization method, it can be divided into attribute extraction and inversion (Ostrander, 1984; Smith and Gidlow 1987, 2003, 2003; Connolly, 1999; Quakenbush et al., 2006; Li et al., 2020). It is a current research trend to

incorporate the reflection coefficient equation with frequency information and rock physics theory to make more use of amplitude and frequency information.

Fluid factor is the characterization of reservoir fluid under the guidance of rock physics theory. The construction of the fluid factor is the key to reservoir fluid identification technology. The fluid factor was initially proposed by Smith and Gidlow (1987). They pointed out that the weighted superposition of P- and S-wave velocity change rates could be used as the response of gas-bearing reservoirs and defined as a fluid factor. Then, using different model parameterization methods, more fluid factors in terms of elastic parameters and P- and S-wave impedance were proposed. For example, Goodway et al. (1997) illustrated that the product of Lambda parameters and density could be used as a fluid factor to identify the fluid anomalies. Gray (1999) and Gray et al. (1999) estimated the Lambda parameters from the pre-stack seismic

E-mail address: zhaoyunzong@yahoo.com (Z.-Y. Zong).

^{*} Corresponding author.

data by eliminating the effect of density, Hedlin (2000) defined the pore modulus following the definition of Murphy et al. (1993), which combined the seismic longitudinal and transverse impedance information. Han and Batzle (2004) gave a simplified form of Gassmann equation and stated that the bulk modulus K_f could be estimated as a fluid factor. Ouakenbush et al. (2006) used the indirect combination of the two impedances to define the Poisson impedance by studying the intersection of longitudinal and transverse wave impedances, and improved the accuracy of fluid identification. Russell et al. (2011) pointed out that the fluid term ρf and Gassmann fluid term f owned better sensitivity to fluid identification, and can be estimated by seismic inversion. Zong et al. (2012) combined the poroelastic theory to represent the fluid term as a function of the P-wave and S-wave modulus, thereby no need for density information from pre-stack seismic data. However, the fluid factors mentioned above are basically traditional fluid factors those are mainly estimated with amplitude information from the seismic data without the consideration of the effect of frequency. And the viscoelasticity of the medium is not well taken into consideration in the definition of the frequency-dependent fluid factors.

Frequency-dependent AVO inversion is a popular method to predict frequency-dependent parameters. Seismic reflectivity equation lays a foundation for AVO inversion. Zoeppritz (1919) established the Zoeppritz equation using plane waves, which comprehensively explained the law of reflection and transmission of incident waves as the beginning of reflectivity equation. However, due to the complexity of Zoeppritz equation, it is not easy to apply directly to parameters inversion. Therefore, different approximate reflectivities of Zoeppritz equation are applied in the field of geophysical exploration (Muskat and Meres, 1940; Koefoed, 1955; Bortfeld, 1961; ; Shuey, 1985; Smith and Gidlow, 1987; Hilterman, 1990Richards and Aki, 1980; Fatti et al., 1994; Goodway et al., 1997; Wang, 1999; Weilian, 2007; Yin et al., 2013), emphasizing the influence of different parameter variations on the reflection amplitude and its sensitivity. Nevertheless, current approximate equations for frequency-dependent AVO inversion do not take into account viscoelastic or velocity dispersion characteristics in the medium (Wilson et al., 2009; ; Wu et al., 2010a; Zhang et al., 2011; Du et al., 2015; Li et al., 2016). Therefore, it is necessary to combine the theory of petrophysics with the reflectivity equation to establish a new frequency-dependent reflection coefficient equation.

Elastic impedance inversion and AVO inversion are two commonly used parameter estimation methods. The former uses elastic impedance equation, the latter uses reflection coefficient and its approximate equation. In terms of elastic impedance inversion, Connolly (1999) proposed an elastic impedance inversion method combining the characteristics of post-stack wave impedance inversion and AVO inversion. Whitcombe (2002) improved it by adopting a normalization method to solve the problem that the numerical dimension varies with the angle. Yin et al. (2010) proposed the elastic impedance equation containing Gassmann's fluid term to directly invert for the high-precision fluid term through elastic impedance inversion. As for AVO inversion, many scholars have proposed different methods based on different perspectives. For example, the Bayesian AVO inversion method (Downton and Lines, 2001; Downton, 2005; Li et al. 2014, 2017), pre-stack inversion method (Zhang et al. 2012, 2018; Liu and Wang, 2013), multi-frequency AVA inversion method for pre-stack gathers (Zhang et al., 2014), frequency-dependent AVO inversion method (Wilson et al., 2009; Wu et al., 2010b; Zhang et al., 2011; Chen et al., 2012), and nonlinear AVO inversion (Pan et al., 2017; Cheng et al., 2018), and so forth. In order to well extract the frequency-dependent viscoelastic solid-liquid decoupling fluid factors, we chose the AVO inversion approach based on pre-stack seismic data.

In this study, a frequency-dependent viscoelastic solid-liquid decoupling fluid factor is established. On this basis, the reflection coefficient equation considering the influence of viscosity is established. Finally, the fluid factor is estimated by frequency-dependent AVO inversion. Through the synthetic and field data examples, it is proved that the proposed fluid factor and its prediction method are helpful to fluid identification.

2. Theory

2.1. Construction of viscoelastic solid-liquid decoupling fluid factor

Based on Biot-Gassmann theory, the solid-liquid coupling effect of pore fluid and the solid-phase effect of rock skeleton are analyzed through petrophysical statistical analysis. The relationship between fluid factor and fluid modulus $K_{\rm f}$ (Han and Batzle, 2004) is

$$f = \frac{\beta^2}{\omega} K_{\rm f} \tag{1}$$

where f is the fluid/pore term, β is the Biot coefficient, φ is the effective porosity of the rock.

In order to consider the viscoelasticity of the medium, we use the Futterman approximation constant Q model. And the P wave complex velocity and the S wave complex velocity in the anelastic medium are

$$\frac{1}{\alpha} = \frac{1}{V_{\rm P}} \left(1 - \frac{1}{\pi Q_{\rm P}} \log \left(\frac{\omega}{\omega_{\rm r}} \right) + \frac{i}{2Q_{\rm P}} \right) \tag{2}$$

and

$$\frac{1}{\beta} = \frac{1}{V_{S}} \left(1 - \frac{1}{\pi Q_{S}} \log \left(\frac{\omega}{\omega_{r}} \right) + \frac{i}{2Q_{S}} \right)$$
 (3)

where α and β are the P wave complex velocity and S wave complex velocity, respectively. V_P and V_S are the P-wave phase velocity and S-wave phase velocity corresponding to the reference frequency ω_Γ , respectively. Q_P and Q_S are the quality factors of P-wave and S-wave, respectively.

Defining $f_{\rm ane}=\rho\alpha^2-\gamma_{\rm dry}^2\rho\beta^2$ where ρ is density, and assuming the ratio of P-wave and S-wave velocity $\gamma_{\rm dry}$ is not affected by attenuation, and $Q_{\rm S}$ is much larger than $Q_{\rm P}$. Thus, the fluid factor of anelastic medium can be expressed as

$$\begin{split} f_{\text{ane}} &= \rho \alpha^2 - \gamma_{\text{dry}}^2 \rho \beta^2 \\ &= \rho V_P^2 \left(1 + \frac{2}{\pi Q_P} \log \left(\frac{\omega}{\omega_r} \right) - \frac{i}{Q_P} \right) \\ &- \gamma_{\text{dry}}^2 \rho V_S^2 \left(1 + \frac{2}{\pi Q_S} \log \left(\frac{\omega}{\omega_r} \right) - \frac{i}{Q_S} \right) \\ &= \rho V_P^2 - \gamma_{\text{dry}}^2 \rho V_S^2 + \rho V_P^2 \left(\frac{2}{\pi Q_P} \log \left(\frac{\omega}{\omega_r} \right) - \frac{i}{Q_P} \right) \\ &- \gamma_{\text{dry}}^2 \rho V_S^2 \left(\frac{2}{\pi Q_S} \log \left(\frac{\omega}{\omega_r} \right) - \frac{i}{Q_S} \right) = f_{\text{ela}} + \Delta f_Q \end{split}$$

$$(4)$$

And $K_{f_{ane}}$ in the anelastic medium is

$$\begin{split} K_{f_{ane}} &= \frac{\varphi}{\beta^2} f_{ane} = \frac{\varphi}{\beta^2} \left(\rho \alpha^2 - \gamma_{dry}^2 \rho \beta^2 \right) \\ &= \frac{\varphi}{\beta^2} \left[\rho V_P^2 \left(1 + \frac{2}{\pi Q_P} \log \left(\frac{\omega}{\omega_r} \right) - \frac{i}{Q_P} \right) \right. \\ &- \gamma_{dry}^2 \rho V_S^2 \left(1 + \frac{2}{\pi Q_S} \log \left(\frac{\omega}{\omega_r} \right) - \frac{i}{Q_S} \right) \right] \\ &= \frac{\varphi}{\beta^2} \left(\rho V_P^2 - \gamma_{dry}^2 \rho V_S^2 \right) + \frac{\varphi}{\beta^2} \left[\rho V_P^2 \left(\frac{2}{\pi Q_P} \log \left(\frac{\omega}{\omega_r} \right) - \frac{i}{Q_P} \right) \right. \\ &- \gamma_{dry}^2 \rho V_S^2 \left(\frac{2}{\pi Q_S} \log \left(\frac{\omega}{\omega_r} \right) - \frac{i}{Q_S} \right) \right] = K_{f_{ela}} + \Delta K_{f_Q} \end{split}$$

$$(5)$$

where $K_{f_{\text{ela}}}$ corresponds to the equivalent fluid bulk modulus in the case of elasticity, and a new disturbance is added in the case of viscoelasticity, namely ΔK_{f_0} .

Equation (5) is the frequency-dependent solid-liquid decoupling fluid factor we define from the viscoelasticity theory.

2.2. Frequency-dependent AVO reflection approximate equation for viscoelastic solid-liquid decoupling fluid factor

Based on the theory of pore elasticity, using theoretical rock physics model and empirical petrophysical model, the effects of rock modulus, pore fluid and pore size on reservoir fluid are fully considered, and the amplitude and frequency anomaly information in seismic data are excavated to construct frequency-dependent pore fluid sensitivity parameters for reservoir fluid identification.

The Aki-Richard approximation in viscoelastic media is

$$R_{\rm pp}^{\rm ane}(\theta,\omega) = \frac{1}{2} \left(1 - \frac{4\sin^2\theta}{\gamma_{\rm sat}^2} \right) \frac{\Delta\rho}{\rho} + \frac{\sec^2\theta}{2} \frac{\Delta\alpha}{\alpha} - \frac{4\sin^2\theta}{\gamma_{\rm sat}^2} \frac{\Delta\beta}{\beta}$$
(6)

Multiplying both sides by $\alpha^2\rho$ to transform the above equation into

$$\begin{split} R_{pp}^{ane}(\theta,\omega) \times \alpha^2 \rho &= \sec^2\theta \frac{\varDelta\alpha \cdot \alpha\rho}{2} - 4\sin^2\theta \cdot \varDelta\beta \cdot \beta\rho + \frac{\varDelta\rho \cdot \alpha^2}{2} \\ &- 2\sin^2\theta \cdot \beta^2 \varDelta\rho \cdot \end{split}$$

With equation (4),

$$\varDelta f_{ane}(\omega) = 2\alpha\rho\varDelta\alpha - 2\gamma_{dry}^2\beta\rho\varDelta\beta + \left(\alpha^2 - \gamma_{dry}^2\beta^2\right)\varDelta\rho, \tag{8}$$

and

$$2\Delta\beta \cdot \beta\rho + \beta^2 \Delta\rho = \frac{1}{\gamma_{\text{dry}}^2} \left(2\Delta\alpha \cdot \alpha\rho + \alpha^2 \Delta\rho - \Delta f_{\text{ane}} \right) \cdot \tag{9}$$

Substituting equation (9) into equation (7) yields,

$$R_{\rm pp}^{\rm ane}(\theta,\omega) \times \alpha^2 \rho = \sec^2 \theta \frac{\Delta \alpha \cdot \alpha \rho}{2} + \frac{\Delta \rho \alpha^2}{2} - \frac{2}{\gamma_{\rm dry}^2} \sin^2 \theta \left(2\Delta \alpha \cdot \alpha \rho + \alpha^2 \Delta \rho - \Delta f_{\rm ane} \right),$$
then,

 $R_{\rm pp}^{\rm ane}(\theta,\omega) \times \alpha^{2}\rho = \frac{2}{\gamma_{\rm dry}^{2}} \sin^{2}\theta \Delta f_{\rm ane} + \left(\frac{\sec^{2}\theta}{2} - \frac{4}{\gamma_{\rm dry}^{2}} \sin^{2}\theta\right) \Delta \alpha \cdot \alpha \rho + \left(\frac{1}{2} - \frac{2}{\gamma_{\rm dry}^{2}} \sin^{2}\theta\right) \alpha^{2} \Delta \rho \cdot$ (11)

Because,

$$\alpha^2 \rho = f_{\text{ane}}(\omega) + \gamma_{\text{dry}}^2 \mu, \tag{12}$$

then,

$$\Delta\alpha \cdot \alpha\rho = \frac{1}{2} \left(\Delta f_{\text{ane}} + \gamma_{\text{dry}}^2 \Delta\mu - \alpha^2 \Delta\rho \right) \cdot \tag{13}$$

Substituting equation (13) into equation (11) yields,

$$\begin{split} R_{pp}^{ane}(\theta,\omega) &= \frac{\sec^2\theta}{4} \frac{\Delta f_{ane}}{\alpha^2\rho} + \left(\frac{\gamma_{dry}^2}{4} \sec^2\theta - 2\sin^2\theta\right) \frac{\Delta\mu}{\alpha^2\rho} \\ &+ \left(\frac{1}{2} - \frac{\sec^2\theta}{4}\right) \frac{\Delta\rho}{\rho} \end{split} \tag{14}$$

With

$$\frac{\Delta f_{\text{ane}}}{\alpha^2 \rho} = \frac{\alpha^2 \rho - \gamma_{\text{dry}}^2 \beta^2 \rho}{\alpha^2 \rho} = 1 - \frac{\gamma_{\text{dry}}^2}{\gamma_{\text{sat}}^2}; \frac{\mu}{\alpha^2 \rho} = \frac{\beta^2 \rho}{\alpha^2 \rho} = \frac{1}{\gamma_{\text{sat}}^2}, \tag{15}$$

getting

$$\frac{1}{\alpha^2 \rho} = \frac{1 - \gamma_{\text{dry}}^2 / \gamma_{\text{sat}}^2}{f_{\text{ane}}} = \frac{1}{\gamma_{\text{sat}}^2 \mu} \tag{16}$$

Substituting equation (16) into equation (14) yields

$$R_{\text{pp}}^{\text{ane}}(\theta,\omega) = \left[\left(\frac{1}{4} - \frac{\gamma_{\text{dry}}^2}{4\gamma_{\text{sat}}^2} \right) \sec^2 \theta \right] \frac{\Delta f_{\text{ane}}}{f_{\text{ane}}} + \left[\frac{\gamma_{\text{dry}}^2}{4\gamma_{\text{sat}}^2} \sec^2 \theta \right] - \frac{2}{\gamma_{\text{sat}}^2} \sin^2 \theta \left[\frac{\Delta \mu}{\mu} + \left[\frac{1}{2} - \frac{\sec^2 \theta}{4} \right] \frac{\Delta \rho}{\rho} \right]$$
(17)

With equation (1),

$$\frac{\Delta f_{\text{ane}}}{f_{\text{ane}}} = \frac{\Delta K_{f_{\text{ane}}}}{K_{f_{\text{ane}}}} + \frac{\Delta \left(\beta^2 \varphi^{-1}\right)}{\left(\beta^2 \varphi^{-1}\right)}$$
(18)

Substituting equation (18) into equation (17) yields,

$$R_{PP}^{\text{ane}}(\theta,\omega) = \left[\left(\frac{1}{4} - \frac{\gamma_{dry}^2}{4\gamma_{sat}^2} \right) \sec^2 \theta \right] \frac{\mathcal{A}K_{f_{\text{ane}}}}{K_{f_{\text{ane}}}} + \left[\left(\frac{\sec^2 \theta}{4} \right) - \frac{2}{\gamma_{\text{sat}}^2} \sin^2 \theta \right] \frac{\mathcal{A}(\beta^2 \varphi^{-1})}{(\beta^2 \varphi^{-1})} + \left[\frac{\gamma_{\text{dry}}^2}{4\gamma_{\text{sat}}^2} \sec^2 \theta \right] - \frac{2}{\gamma_{\text{sat}}^2} \sin^2 \theta \frac{\Delta \mu_{\text{m}}}{\mu_{\text{m}}} + \left[\frac{1}{2} - \frac{\sec^2 \theta}{4} \right] \frac{\Delta \rho}{\rho},$$

$$(19)$$

where

$$\mu_{\rm m} = \frac{\varphi}{\beta^2} \mu,\tag{20}$$

 $\gamma_{\rm sat}$ is the ratio of P-wave velocity and S-wave velocity in dry rock, $\gamma_{\rm dry}$ is the ratio of S-wave velocity and P-wave velocity in fluid-saturated rock, $K_{\rm fane}$ is a fluid modulus which is influenced by the fluid content. β is the Biot coefficient, φ is the effective porosity of the rock, $\mu_{\rm m}$ and $\beta^2 \varphi^{-1}$ are built-up terms without specific physical meaning, which lead to the simplification of the proposed reflectivity equation, and they are addressed as the shear modulus of the rock matrix and porosity divided by the square of Biot coefficient, respectively.

Considering the attenuation factor in the Futterman approximation constant Q model

$$\gamma_{\text{sat}}^{2} = \frac{\alpha^{2}}{\beta^{2}} = \frac{V_{P}^{2}}{V_{S}^{2}} \frac{1}{\left[1 - \frac{1}{\pi Q_{P}} \log\left(\frac{\omega}{\omega_{r}}\right) + \frac{i}{2Q_{P}}\right]^{2}}$$

$$\approx \frac{V_{P}^{2}}{V_{S}^{2}} \left[1 + \frac{2}{\pi Q_{P}} \log\left(\frac{\omega}{\omega_{r}}\right) - \frac{i}{Q_{P}}\right] \cdot$$
(21)

and

$$\frac{1}{\gamma_{sat}^{\prime 2}} = \frac{\beta^{2}}{\alpha^{2}} = \frac{V_{S}^{2}}{V_{P}^{2}} \left[1 - \frac{1}{\pi Q_{P}} \log \left(\frac{\omega}{\omega_{r}} \right) + \frac{i}{2Q_{P}} \right]^{2}$$

$$\approx \frac{V_{S}^{2}}{V_{P}^{2}} \left[1 - \frac{2}{\pi Q_{P}} \log \left(\frac{\omega}{\omega_{r}} \right) + \frac{i}{Q_{P}} \right]$$

$$= \frac{1}{\gamma_{sat}^{2}} \left[1 - \frac{2}{\pi Q_{P}} \log \left(\frac{\omega}{\omega_{r}} \right) + \frac{i}{Q_{P}} \right] \cdot \tag{22}$$

Assuming that the P- and S- wave velocity ratio of the dry rock is not affected by the attenuation, substituting equation (22) into equation (19) yields

$$\begin{split} R_{\mathrm{PP}}^{\mathrm{ane}}(\theta,\omega) &\approx \left[\left(1 - \frac{\gamma_{\mathrm{dry}}^2}{\gamma_{\mathrm{sat}}^2} \right) \frac{\sec^2 \theta}{4} \right] \frac{\Delta K_{f_{\mathrm{ane}}}}{K_{f_{\mathrm{fane}}}} + \left(\frac{\gamma_{\mathrm{dry}}^2}{4\gamma_{\mathrm{sat}}^2} \sec^2 \theta \right) \\ &- \frac{2}{\gamma_{\mathrm{sat}}^2} \sin^2 \theta \right) \frac{\Delta \mu_{\mathrm{m}}}{\mu_{\mathrm{m}}} + \left[\frac{\sec^2 \theta}{4} - \frac{2}{\gamma_{\mathrm{sat}}^2} \sin^2 \theta \right] \frac{\Delta \left(\beta^2 \varphi^{-1} \right)}{\beta^2 \varphi^{-1}} + \left[\frac{1}{2} \right] \\ &- \frac{\sec^2 \theta}{4} \right] \frac{\Delta \rho}{\rho} \approx \left[\left(1 - \frac{\gamma_{\mathrm{dry}}^2}{\gamma_{\mathrm{sat}}^2} \left(1 - \frac{2}{\pi Q_{\mathrm{p}}} \log \left(\frac{\omega}{\omega_{\mathrm{r}}} \right) \right) \right. \\ &+ \frac{i}{Q_{\mathrm{p}}} \right) \left. \right) \frac{\sec^2 \theta}{4} \right] \frac{\Delta K_{f_{\mathrm{ane}}}}{K_{f_{\mathrm{fane}}}} + \left(\frac{\gamma_{\mathrm{dry}}^2}{4\gamma_{\mathrm{sat}}^2} \sec^2 \theta - \frac{2}{\gamma_{\mathrm{sat}}^2} \sin^2 \theta \right) \left(1 \right. \\ &- \frac{2}{\pi Q_{\mathrm{p}}} \log \left(\frac{\omega}{\omega_{\mathrm{r}}} \right) + \frac{i}{Q_{\mathrm{p}}} \right) \frac{\Delta \mu_{\mathrm{m}}}{\mu_{\mathrm{m}}} + \left[\frac{\sec^2 \theta}{4} - \frac{2}{\gamma_{\mathrm{sat}}^2} \left(1 \right. \\ &- \frac{2}{\pi Q_{\mathrm{p}}} \log \left(\frac{\omega}{\omega_{\mathrm{r}}} \right) + \frac{i}{Q_{\mathrm{p}}} \right) \sin^2 \theta \left. \right] \frac{\Delta \left(\beta^2 \varphi^{-1} \right)}{\beta^2 \varphi^{-1}} + \left[\frac{1}{2} - \frac{\sec^2 \theta}{4} \right] \frac{\Delta \rho}{\rho} \end{split}$$

The viscoelastic P-wave reflection coefficient contains an imaginary part. Due to its weak anelastic property, we observe that the imaginary part is much smaller than the real part, and ignore it

Table 1Parameters used by Futterman approximation constant Q model.

	V _P , m/s	V _S , m/s	ρ , kg/m ³	Q_{P1}	Q_{P2}	Qs
Medium	6230	3170	2730	10	20	120

to get the reflection coefficient (Chen et al., 2018).

$$\begin{split} R_{PP}^{ane}(\theta,\omega) &= \left[\left(1 - \frac{\gamma_{dry}^2}{\gamma_{sat}^2} \left(1 - \frac{2}{\pi Q_P} log \left(\frac{\omega}{\omega_r} \right) \right) \right) \frac{sec^2 \theta}{4} \right] \frac{\Delta K_{f_{ane}}}{K_{f_{ane}}} \\ &+ \left(\frac{\gamma_{dry}^2}{4\gamma_{sat}^2} sec^2 \theta - \frac{2}{\gamma_{sat}^2} sin^2 \theta \right) \left(1 \right. \\ &- \frac{2}{\pi Q_P} log \left(\frac{\omega}{\omega_r} \right) \right) \frac{\Delta \mu_m}{\mu_m} + \left[\frac{sec^2 \theta}{4} - \frac{2}{\gamma_{sat}^2} \left(1 \right. \right. \\ &- \frac{2}{\pi Q_P} log \left(\frac{\omega}{\omega_r} \right) \right) sin^2 \theta \right] \frac{\Delta \left(\beta^2 \varphi^{-1} \right)}{\beta^2 \varphi^{-1}} + \left[\frac{1}{2} \right. \\ &- \frac{sec^2 \theta}{4} \right] \frac{\Delta \rho}{\rho} \end{split}$$

This equation is a solid-liquid decoupling fluid factor reflection characteristic equation in the case of viscoelastic medium. Simplify equation (24) to

$$\begin{split} R_{\mathrm{PP}}^{\mathrm{ane}}(\theta,\omega) &= a(\theta,\omega) \frac{\varDelta K_{f_{\mathrm{ane}}}}{K_{f_{\mathrm{ane}}}} + b(\theta,\omega) \frac{\varDelta \mu_{\mathrm{m}}}{\mu_{\mathrm{m}}} + c(\theta) \frac{\varDelta \left(\beta^{2} \varphi^{-1}\right)}{\beta^{2} \varphi^{-1}} \\ &+ d(\theta) \frac{\varDelta \rho}{\rho} \end{split} \tag{25}$$

where

$$\begin{split} a(\theta,\omega) &= \left(1 - \frac{\gamma_{\text{dry}}^2}{\gamma_{\text{sat}}^2} \left(1 - \frac{2}{\pi Q_P} \log\left(\frac{\omega}{\omega_r}\right)\right)\right) \frac{\sec^2 \theta}{4} \\ b(\theta,\omega) &= \left(\frac{\gamma_{\text{dry}}^2}{4\gamma_{\text{sat}}^2} \sec^2 \theta - \frac{2}{\gamma_{\text{sat}}^2} \sin^2 \theta\right) \left(1 - \frac{2}{\pi Q_P} \log\left(\frac{\omega}{\omega_r}\right)\right) \\ c(\theta) &= \frac{\sec^2 \theta}{4} - \frac{2}{\gamma_{\text{sat}}^2} \left(1 - \frac{2}{\pi Q_P} \log\left(\frac{\omega}{\omega_r}\right)\right) \sin^2 \theta \\ d(\theta) &= \frac{1}{2} - \frac{\sec^2 \theta}{4} \end{split}$$
 (26)

Based on the viewpoint of dispersion proposed by Chapman et al. (2002), it is assumed that the reflection coefficient changes with frequency due to the difference in dispersion properties on both sides of the interface of the subsurface medium. If the velocity dispersion causes the P- and S-wave velocities to change with frequency, then $\Delta K_{f_{\rm ane}}/K_{f_{\rm ane}}$ and $\Delta \mu_{\rm m}/\mu_{\rm m}$ also change with frequency. By considering the dispersion effect, equation (9) can be expressed as a function of incident angle and frequency, and the medium density will not change with frequency, the following equation

$$\begin{split} R_{\mathrm{PP}}^{\mathrm{ane}}(\theta,\omega) &= a(\theta,\omega) \frac{\varDelta K_{f_{\mathrm{ane}}}}{K_{f_{\mathrm{ane}}}}(\omega) + b(\theta,\omega) \frac{\varDelta \mu_{\mathrm{m}}}{\mu_{\mathrm{m}}}(\omega) + c(\theta) \frac{\varDelta \left(\beta^{2} \varphi^{-1}\right)}{\beta^{2} \varphi^{-1}} \\ &+ d(\theta) \frac{\varDelta \rho}{\rho} \end{split} \tag{27}$$

The frequency-dependent characteristic of the relative variation of the fluid factor and the shear modulus changes approximately

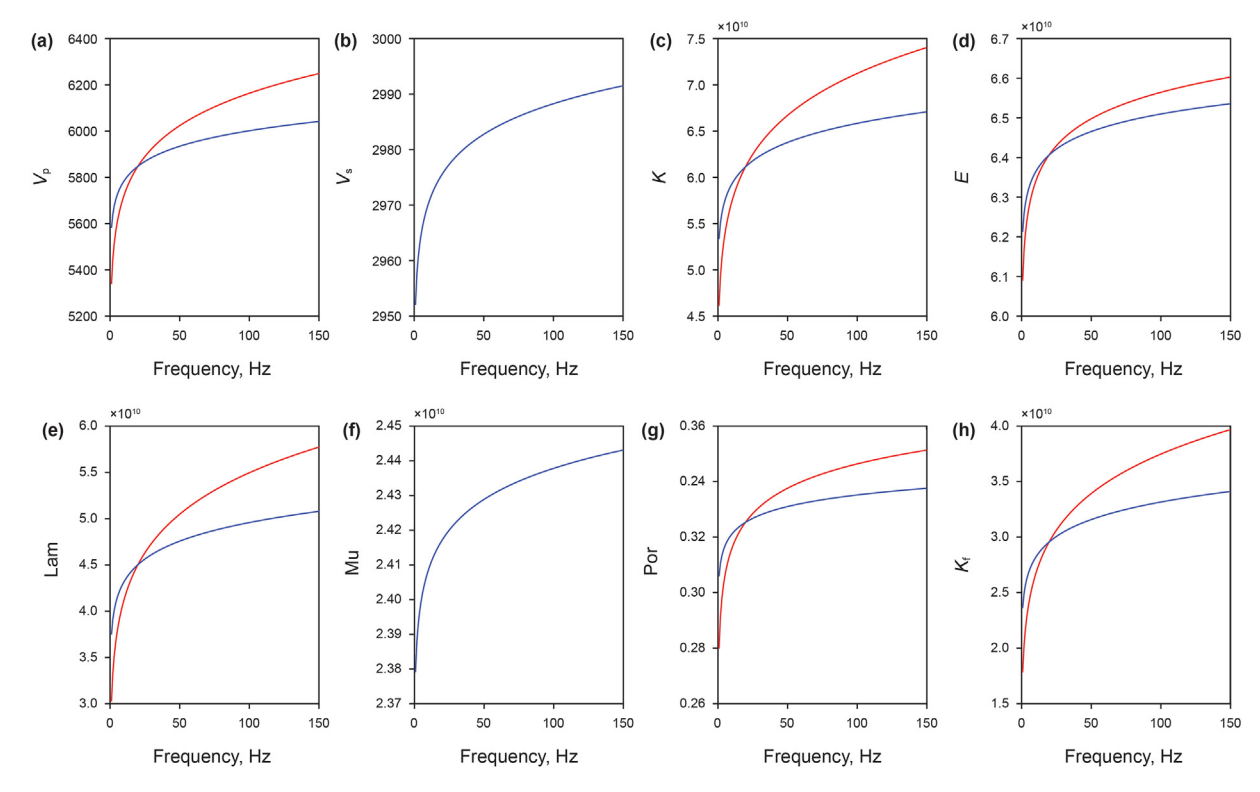


Fig. 1. Frequency-dependent characteristics of approximation constant Q model for elastic modulus (the red line is the elastic modulus at $Q_P = 10$ and the blue line is the elastic modulus at $Q_P = 20$). (a). V_P ; (b). V_S ; (c). K; (d). E; (e). λ ; (f). μ ; (g). σ ; (h). $K_{f_{max}}$.

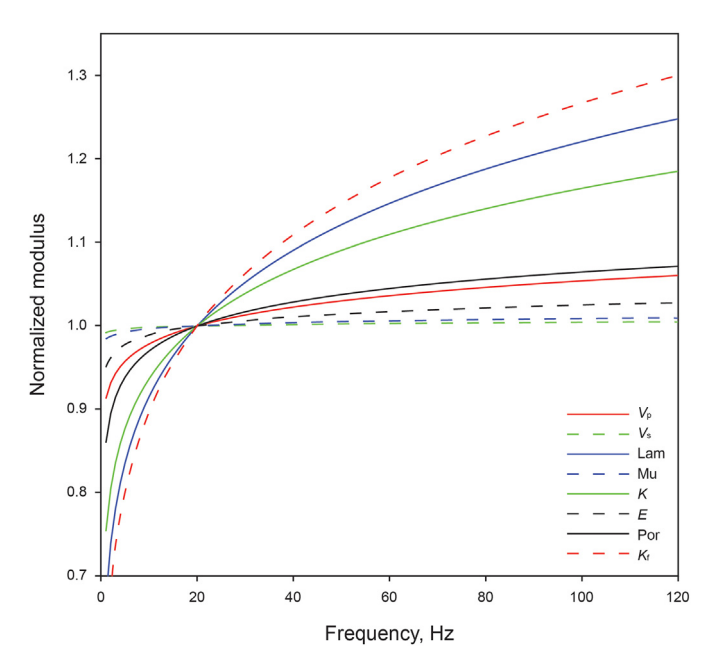


Fig. 2. Comparative analysis of frequency-dependent gradient of frequency-dependent elastic parameters in the approximation constant Q model.

Table 2Parameters used for frequency-dependent P-wave reflection coefficient.

	V _P , m/s	V _S , m/s	ρ, kg/m ³	$Q_{\rm P}$	Qs	ω _r , Hz
Medium 1	2800	1160	2100	10	∞	20
Medium 2	2300	1500	1930	∞	∞	20

linearly in the dispersion region. Therefore, $\frac{AK_{\mathrm{fane}}}{K_{\mathrm{fane}}}(\omega)$ and $\frac{\Delta\mu_{\mathrm{m}}}{\mu_{\mathrm{m}}}(\omega)$ can be expanded into Taylor series form under the reference frequency ω_0 , and the high-order term is ignored to obtain the first-order approximation of the reflection coefficient,

$$\begin{split} R_{\mathrm{PP}}^{\mathrm{ane}}(\theta,\omega) &= a(\theta,\omega_0) \frac{\varDelta K_{f_{\mathrm{ane}}}}{K_{f_{\mathrm{ane}}}}(\omega_0) + (\omega - \omega_0) a(\theta,\omega) \frac{d}{d\omega} \left(\frac{\varDelta K_{f_{\mathrm{ane}}}}{K_{f_{\mathrm{ane}}}}\right) \\ &+ b(\theta,\omega_0) \frac{\varDelta \mu_{\mathrm{m}}}{\mu_{\mathrm{m}}}(\omega_0) + (\omega - \omega_0) b(\theta,\omega) \frac{d}{d\omega} \left(\frac{\varDelta \mu_{\mathrm{m}}}{\mu_{\mathrm{m}}}\right) \\ &+ c(\theta) \frac{\varDelta \left(\beta^2 \varphi^{-1}\right)}{\beta^2 \varphi^{-1}} + d(\theta) \frac{\varDelta \rho}{\rho} \end{split} \tag{28}$$

To simplify equation (28), the relative change in $K_{f_{ane}}$ and μ_{m} which is the value of the first derivative of the frequency at ω_{0} are,

$$I_{K_{fane}} = \frac{d}{d\omega} \left(\frac{\Delta K_{f_{ane}}}{K_{f_{ane}}} \right); \quad I_{\mu_{m}} = \frac{d}{d\omega} \left(\frac{\Delta \mu_{m}}{\mu_{m}} \right)$$
 (29)

And the reflection coefficient at the reference frequency ω_0 is,

$$\begin{split} R_{\mathrm{PP}}^{\mathrm{ane}}(\theta,\omega_{0}) &= a(\theta,\omega_{0}) \frac{\varDelta K_{f_{\mathrm{ane}}}}{K_{f_{\mathrm{ane}}}}(\omega_{0}) + b(\theta,\omega_{0}) \frac{\varDelta \mu_{\mathrm{m}}}{\mu_{\mathrm{m}}}(\omega_{0}) \\ &+ c(\theta) \frac{\varDelta \left(\beta^{2} \varphi^{-1}\right)}{\beta^{2} \varphi^{-1}} + d(\theta) \frac{\varDelta \rho}{\rho} \end{split} \tag{30}$$

Substituting equations (29) and (30) into equation (28), and

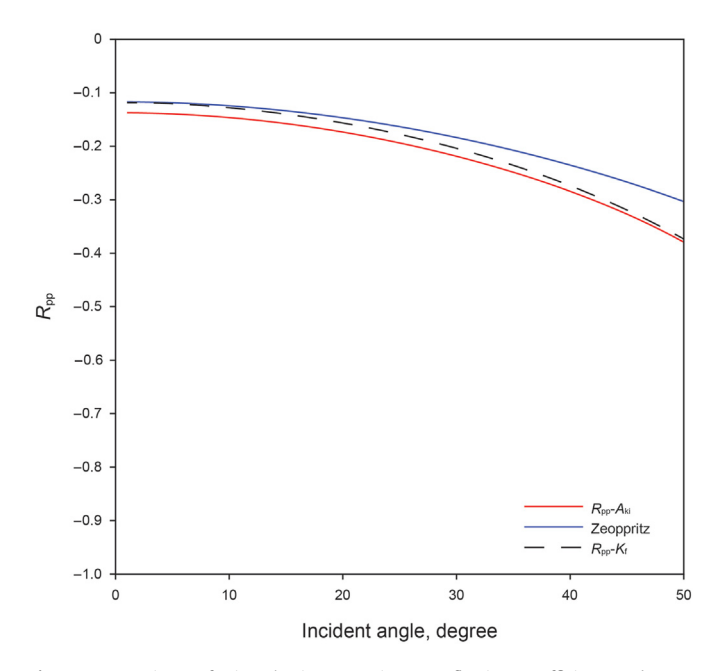


Fig. 3. Comparison of viscoelastic approximate reflection coefficient and exact reflection coefficient equation at reference frequency $\omega_r=20$ Hz.

defining $\Delta \omega = \omega - \omega_0$, the original equation changes to,

$$R_{\rm pp}^{\rm ane}(\theta,\omega) = R_{\rm pp}^{\rm ane}(\theta,\omega_0) + a(\theta,\omega)I_{K_{\rm fane}}\Delta\omega + b(\theta,\omega)I_{\mu_{\rm m}}\Delta\omega \tag{31}$$

Defining
$$\Delta R_{\rm pp}^{\rm ane}(\theta,\omega) = R_{\rm pp}^{\rm ane}(\theta,\omega) - R_{\rm pp}^{\rm ane}(\theta,\omega_0)$$
,

$$\Delta R_{\rm PP}^{\rm ane}(\theta,\omega) = a(\theta,\omega) I_{K_{\rm free}} \Delta \omega + b(\theta,\omega) I_{\mu_{\rm m}} \Delta \omega \tag{32}$$

where $I_{K_{\rm fane}}$ and $I_{\mu_{\rm m}}$ are the frequency-dependent characteristics to be inverted, and they can be used as fluid factors for fluid identification.

2.3. Frequency-dependent AVO inversion method for viscoelastic solid-liquid decoupling fluid factor

In the cases of two offsets (θ_1 and θ_2), two sampling points, and two frequencies (ω_1 and ω_2), equation (32) in matrix form is,

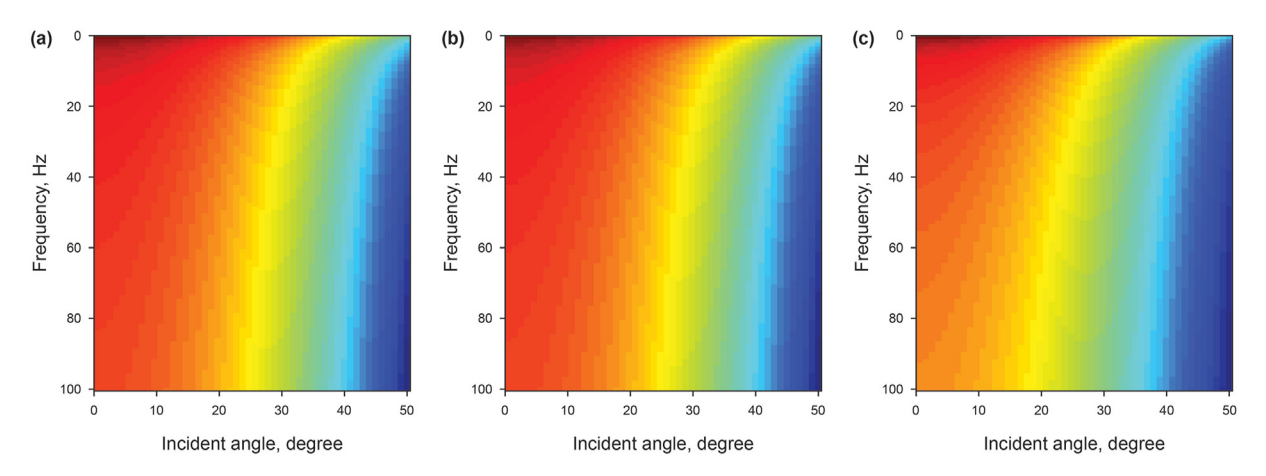


Fig. 4. Accuracy analysis of frequency-dependent reflection coefficient when $Q_{P1}=10$, $Q_{S1}=\infty$; $Q_{P2}=\infty$, $Q_{S2}=\infty$. (a). the exact Zoeppritz equation; (b). the Aki-Rhichards approximation equation; (c). the approximate equation for solid-liquid decoupling fluid factor.

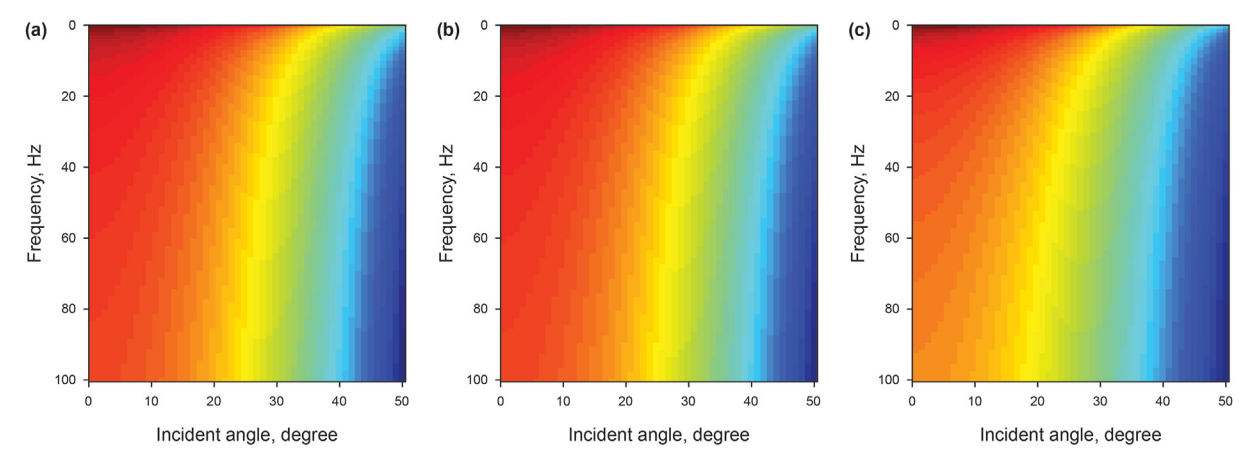


Fig. 5. Accuracy analysis of frequency-dependent reflection coefficient when $Q_{P1}=5$, $Q_{S1}=\infty$; $Q_{P2}=\infty$, $Q_{S2}=\infty$. (a). the exact Zoeppritz equation; (b). the Aki-Rhichards approximation equation; (c). the approximate equation for solid-liquid decoupling fluid factor.

Z.-Y. Zong, Y.-W. Feng, X.-Y. Yin et al. Petroleum Science 18 (2021) 1047–1058

$$\begin{bmatrix} \Delta R^{1}(\theta_{1},\omega_{1}) \\ \Delta R^{2}(\theta_{1},\omega_{1}) \\ \Delta R^{1}(\theta_{2},\omega_{1}) \\ \Delta R^{2}(\theta_{2},\omega_{1}) \\ \Delta R^{2}(\theta_{2},\omega_{1}) \\ \Delta R^{2}(\theta_{2},\omega_{1}) \\ \Delta R^{1}(\theta_{1},\omega_{2}) \\ \Delta R^{2}(\theta_{1},\omega_{2}) \\ \Delta R^{2}(\theta_{1},\omega_{2}) \\ \Delta R^{2}(\theta_{2},\omega_{2}) \\ \Delta R^{2}(\theta_{2},\omega_{2}) \\ \Delta R^{2}(\theta_{2},\omega_{2}) \end{bmatrix} = \begin{bmatrix} (\omega_{1} - \omega_{0})a(\theta_{1},\omega_{1}) & 0 & (\omega_{1} - \omega_{0})b(\theta_{1},\omega_{1}) & 0 \\ 0 & (\omega_{1} - \omega_{0})a(\theta_{2},\omega_{1}) & 0 & (\omega_{1} - \omega_{0})b(\theta_{2},\omega_{1}) & 0 \\ (\omega_{2} - \omega_{0})a(\theta_{1},\omega_{2}) & 0 & (\omega_{2} - \omega_{0})b(\theta_{1},\omega_{2}) & 0 \\ 0 & (\omega_{2} - \omega_{0})a(\theta_{2},\omega_{2}) & 0 & (\omega_{2} - \omega_{0})b(\theta_{2},\omega_{2}) & 0 \\ 0 & (\omega_{2} - \omega_{0})a(\theta_{2},\omega_{2}) & 0 & (\omega_{2} - \omega_{0})b(\theta_{2},\omega_{2}) & 0 \\ 0 & (\omega_{2} - \omega_{0})a(\theta_{2},\omega_{2}) & 0 & (\omega_{2} - \omega_{0})b(\theta_{2},\omega_{2}) \end{bmatrix} \begin{bmatrix} I_{K_{\text{Jane}}}^{1} \\ I_{\mu_{\text{m}}}^{1} \\ I_{\mu_{\text{m}}}^{2} \\ I_{\mu_{\text{m}}}^{2} \end{bmatrix}$$

$$(33)$$

Extending to case of m offsets, n samples and l frequencies, and the matrix is,

$$\begin{bmatrix}
\Delta \mathbf{R}_{1}^{1} \\
\Delta \mathbf{R}_{2}^{1} \\
\vdots \\
\Delta \mathbf{R}_{m}^{1} \\
\Delta \mathbf{R}_{2}^{2}
\end{bmatrix} = \begin{bmatrix}
\Delta \mathbf{F}^{1} a_{1}^{1} & \Delta \mathbf{F}^{1} b_{1}^{1} \\
\Delta \mathbf{F}^{1} a_{2}^{1} & \Delta \mathbf{F}^{1} b_{2}^{1} \\
\vdots & \vdots \\
\Delta \mathbf{F}^{1} a_{m}^{1} & \Delta \mathbf{F}^{1} b_{m}^{1} \\
\Delta \mathbf{F}^{2} a_{1}^{2} & \Delta \mathbf{F}^{2} b_{1}^{2} \\
\vdots & \vdots \\
\Delta \mathbf{F}^{2} a_{m}^{2} & \Delta \mathbf{F}^{2} b_{m}^{2} \\
\vdots & \vdots \\
\Delta \mathbf{F}^{l} a_{m}^{l} & \Delta \mathbf{F}^{l} b_{m}^{l}
\end{bmatrix}$$

$$(34)$$

where, $\Delta \mathbf{R}^i_{ii}$ $(i=1,\,2,\,\cdots,\,l;\,ii=1,\,2,\,\cdots m)$ represents the ii-th offset, the data column vector of the total n sampling points corresponding to the frequency ω_i . $\Delta \mathbf{F}^i$ $(i=1,\,2,\,\cdots,\,l)$ is the oblique diagonal matrix formed by the difference between the frequencies ω_i and ω_0 . \mathbf{a}^i_{ii} $(i=1,\,2,\,\cdots,\,l;\,ii=1,\,2,\,\cdots m)$ is the ii-th offset, and the oblique diagonal coefficient matrix corresponding to $I_{K_{\mathrm{Jane}}}$ when the frequency is ω_i . \mathbf{b}^i_{ii} $(i=1,\,2,\,\cdots,\,l;\,ii=1,\,2,\,\cdots m)$ is the ii-th offset, the oblique diagonal coefficient matrix corresponding to $I_{\mu_{\mathrm{m}}}$ when the frequency is ω_i . $I_{K_{\mathrm{Jane}}}$ and $I_{\mu_{\mathrm{m}}}$ respectively represent the frequency-dependent characteristics to be inverted.

Convoluting with seismic wavelets,

$$\begin{bmatrix} \mathbf{D}_{1}^{1} \\ \mathbf{D}_{2}^{1} \\ \vdots \\ \mathbf{D}_{m}^{1} \\ \mathbf{D}_{1}^{2} \\ \vdots \\ \mathbf{D}_{m}^{2} \\ \vdots \\ \mathbf{W}_{1}\Delta\mathbf{F}^{1}a_{1}^{1} & \mathbf{W}_{1}\Delta\mathbf{F}^{1}b_{1}^{1} \\ \mathbf{W}_{1}\Delta\mathbf{F}^{1}a_{2}^{1} & \mathbf{W}_{1}\Delta\mathbf{F}^{1}b_{m}^{1} \\ \mathbf{W}_{2}\Delta\mathbf{F}^{2}a_{1}^{2} & \mathbf{W}_{2}\Delta\mathbf{F}^{2}b_{1}^{2} \\ \vdots \\ \mathbf{W}_{2}\Delta\mathbf{F}^{2}a_{m}^{2} & \mathbf{W}_{2}\Delta\mathbf{F}^{2}b_{m}^{2} \\ \vdots \\ \mathbf{W}_{l}\Delta\mathbf{F}^{l}a_{m}^{l} & \mathbf{W}_{l}\Delta\mathbf{F}^{l}b_{m}^{l} \end{bmatrix} \begin{bmatrix} \mathbf{I}_{K_{fane}} \\ \mathbf{I}_{\mu_{m}} \end{bmatrix}$$

$$(35)$$

where \mathbf{D}_{ii}^{i} ($i=1, 2, \cdots, l$; $ii=1, 2, \cdots, m$) is the ii-th offset, the frequency ω_{i} and the frequency ω_{0} corresponding to the column vector of the amplitude information. \mathbf{W}_{i} ($i=1, 2, \cdots, l$) is the wavelet matrix corresponding to the frequency ω_{i} , and the wavelet matrices are different at different frequencies.

Defining **D**, **m**, and **G** as,

$$\mathbf{D} = \begin{bmatrix} \mathbf{D}_{1}^{1} \\ \mathbf{D}_{2}^{1} \\ \vdots \\ \mathbf{D}_{m}^{1} \\ \mathbf{D}_{1}^{2} \\ \vdots \\ \mathbf{D}_{m}^{2} \\ \vdots \\ \mathbf{D}_{m}^{l} \end{bmatrix}$$

$$(36)$$

$$\mathbf{m} = \begin{bmatrix} \mathbf{I}_{K_{f_{ane}}} \\ \mathbf{I}_{\mu_m} \end{bmatrix} \tag{37}$$

$$\mathbf{G} = \begin{bmatrix} \mathbf{W}_{1} \Delta \mathbf{F}^{1} \mathbf{a}_{1}^{1} & \mathbf{W}_{1} \Delta \mathbf{F}^{1} \mathbf{b}_{1}^{1} \\ \mathbf{W}_{1} \Delta \mathbf{F}^{1} \mathbf{a}_{2}^{1} & \mathbf{W}_{1} \Delta \mathbf{F}^{1} \mathbf{b}_{2}^{1} \\ \vdots & \vdots \\ \mathbf{W}_{1} \Delta \mathbf{F}^{1} \mathbf{a}_{m}^{1} & \mathbf{W}_{1} \Delta \mathbf{F}^{1} \mathbf{b}_{m}^{1} \\ \mathbf{W}_{2} \Delta \mathbf{F}^{2} \mathbf{a}_{1}^{2} & \mathbf{W}_{2} \Delta \mathbf{F}^{2} \mathbf{b}_{1}^{2} \\ \vdots & \vdots \\ \mathbf{W}_{2} \Delta \mathbf{F}^{2} \mathbf{a}_{m}^{2} & \mathbf{W}_{2} \Delta \mathbf{F}^{2} \mathbf{b}_{m}^{2} \\ \vdots & \vdots \\ \mathbf{W}_{l} \Delta \mathbf{F}^{l} \mathbf{a}_{m}^{l} & \mathbf{W}_{l} \Delta \mathbf{F}^{l} \mathbf{b}_{m}^{l} \end{bmatrix}$$

$$(38)$$

Substituting equations (36)–(38) into equation (35) yields

$$\mathbf{D} = \mathbf{Gm} \tag{39}$$

Under the Bayesian framework, the posterior probability distribution of the parameters θ to be inverted is

$$p\left(\theta \middle| x\right) = \frac{p(\theta)p(x|\theta)}{\int p(x|\theta)d\theta} \propto p\left(\theta\right)p\left(x\middle|\theta\right) \tag{40}$$

where, θ is the parameter to be inverted, x is the observed sample, $p(\theta|x)$ is the posterior probability density, $p(\theta)$ is the prior probability density, and $p(x|\theta)$ is the likelihood function.

The Bayesian estimation estimates $\overline{\mathbf{m}}'$ by pre-stack partial angle superimposed gather data D with noise. Assuming that the likelihood function obeys the Cauchy distribution as

$$p(\overline{\mathbf{m}}') = \frac{1}{(\pi \sigma_m)^M} \prod_{i=1}^M \left[\frac{1}{1 + \overline{\mathbf{m}}_i'^2 / \sigma_m^2} \right]$$
(41)

where M is the number of model parameters, σ_m^2 is the variance of the parameters to be inverted, and the posterior probability distribution of the parameters is,

$$p(\overline{\mathbf{m}}', \sigma_n | \mathbf{d}) \propto \prod_{i=1}^{M} \left[\frac{1}{1 + \overline{\mathbf{m}}_i'^2 / \sigma_m^2} \right] \cdot \exp \left[-\frac{\left(\mathbf{D} - \overline{\mathbf{G}}' \overline{\mathbf{m}}' \right)^{\mathrm{T}} \left(\mathbf{D} - \overline{\mathbf{G}}' \overline{\mathbf{m}}' \right)}{2\sigma_n^2} \right]$$
(42)

Maximizing the posterior probability distribution (42) gives the initial objective function as,

$$F(\overline{\mathbf{m}}') = \left(\mathbf{D} - \overline{\mathbf{G}}'\overline{\mathbf{m}}'\right)^{\mathsf{T}} \left(\mathbf{D} - \overline{\mathbf{G}}'\overline{\mathbf{m}}'\right) + 2\sigma_n^2 \sum_{i=1}^{M} \ln\left(1 + \overline{\mathbf{m}}_i'^2 / \sigma_m^2\right)$$
(43)

Adding the initial model constraint yields,

$$F(\overline{\mathbf{m}}') = \left(\mathbf{D} - \overline{\mathbf{G}}'\overline{\mathbf{m}}'\right)^{\mathrm{T}} \left(\mathbf{D} - \overline{\mathbf{G}}'\overline{\mathbf{m}}'\right) + 2\sigma_{n}^{2}$$

$$\times \sum_{i=1}^{M} \ln\left(1 + \overline{\mathbf{m}}_{i}'^{2} / \sigma_{m}^{2}\right) + S$$
(44)

where,

$$S = \lambda_{K_{\text{fane}}} \left(\mathbf{\eta}_{I_{K_{\text{fane}}}} - P \mathbf{I}_{K_f} \right)^{\text{T}} \left(\mathbf{\eta}_{I_{K_{\text{fane}}}} - P \mathbf{I}_{K_{\text{fane}}} \right)$$

$$+ \lambda_{\mu_{\text{m}}} \left(\mathbf{\eta}_{I_{\mu_{\text{m}}}} - P \mathbf{I}_{\mu_{m}} \right)^{\text{T}} \left(\mathbf{\eta}_{I_{\mu_{\text{m}}}} - P \mathbf{I}_{\mu_{m}} \right)$$

$$(45)$$

where, $\lambda_{K_{fane}}$ and λ_{μ_m} are constraint factors, P is $\int_{t_0}^t d\tau$, $\eta_{I_{K_{fane}}} = \frac{1}{2} \ln(\mathbf{I}_{\mathbf{K}_{fane}}/\mathbf{I}_{\mathbf{K}_{f_0}})$, $\eta_{I_{\mu_m}} = \frac{1}{2} \ln(\mathbf{I}_{\mu_m}/\mathbf{I}_{\mu_{m_0}})$.

Equation (44) has weak nonlinearity and can be optimized by an iterative weighted least squares (IRLS) algorithm (Dai et al., 2018).

3. Synthetic examples

3.1. Sensitivity evaluation of frequency-dependent solid-liquid decoupling fluid factor

Based on the Futterman approximation constant Q model, the variation of elastic parameters with frequency in anelastic medium is simulated, and the sensitivity of elastic parameters with frequency is compared. The approximation constant Q model

parameters are displayed in Table 1. The P-wave complex velocity and the S-wave complex velocity in anelastic medium are obtained with those parameters, and the elastic parameters are further calculated according to the conversion relation between the elastic parameters, and the variation characteristics of the elastic parameters with frequency are finally calculated.

In order to clarify the gradient of the elastic parameters with frequency, Fig. 1 displays the frequency-dependent characteristics of approximation constant Q model for the Lambda parameter λ , shear modulus μ , P-wave velocity $V_{\rm P}$, S-wave velocity $V_{\rm S}$, frequency-dependent viscoelastic solid-liquid decoupling fluid factor $K_{f_{\rm lne}}$, volume modulus K, Young's modulus E, and Poisson's ratio σ , respectively. It can be seen from the figure that all elastic parameters change with frequency.

Fig. 2 shows the comparison of the frequency-dependent degree of the normalized elastic parameters. It can be seen that the frequency dispersion of the frequency-dependent solid-liquid decoupling fluid factor in viscoelastic media is the largest among many elastic parameters. Therefore, the frequency-dependent solid-liquid decoupling fluid factor is used as a sensitive parameter for reservoir fluid identification, and helps to enhance the reliability and stability of fluid identification.

3.2. Accuracy analysis of characteristic equations of seismic frequency response of solid-liquid decoupling fluid factor

In order to study the influence of anelastic characteristics on the reflection coefficient, the following parameters are used to compare the difference between the reflection coefficient of viscoelastic medium and that of elastic medium as in Table 2. As shown in Fig. 3, the viscoelastic approximation reflection coefficient at the reference frequency $\omega_{\rm r}=20$ Hz is compared with the exact reflection coefficient equation. It can be seen that the reflection characteristics of the solid-liquid decoupling fluid factor in viscoelastic medium are approximately consistent with the Aki-Rhichards approximation equation in the corresponding viscoelastic medium.

Figs. 4 and 5 illustrate the viscoelastic approximation reflection coefficients and the exact reflection coefficients varying with frequency and incident angle. It can be seen that in viscoelastic media, the exact Zoeppritz equation, the Aki-Rhichards approximation equation, and the solid-liquid decoupling fluid factor approximation equation are basically consistent with the trends of angle and frequency, verifying the accuracy of the solid-liquid decoupling fluid factor approximation equation.

3.3. Synthetic and field data examples

In order to verify the feasibility of the frequency-dependent solid-liquid decoupling fluid factor AVO inversion method, well logging curves are used for synthetic examples. The original $K_{f_{\rm ane}}$ and $\mu_{\rm m}$ of a well are displayed in blue in Fig. 6. The pre-stack seismic data is obtained by using the convolution of the exact reflection coefficient equation and the seismic wavelet (Ricker wavelet). Then we use the inversion method proposed in this paper to estimate parameters. In Fig. 6, the estimated $K_{f_{\rm ane}}$ and $\mu_{\rm m}$ of the well are displayed in red and the initial model is displayed in green, respectively. From Fig. 6(a), the relative prediction errors of these parameters are small. To further verify the stability of the inversion, we add random Gaussian noise to the synthetic seismic trace with the S/N is 2:1, 5:1 and 10:1, respectively. It can be seen that we can still get better inversion results with moderate noise.

Field data example in eastern China is utilized to verify the feasibility and reliability of the inversion method. Fig. 7 shows the pre-stack angled partial stacking seismic data profile extracted

Z.-Y. Zong, Y.-W. Feng, X.-Y. Yin et al. Petroleum Science 18 (2021) 1047–1058

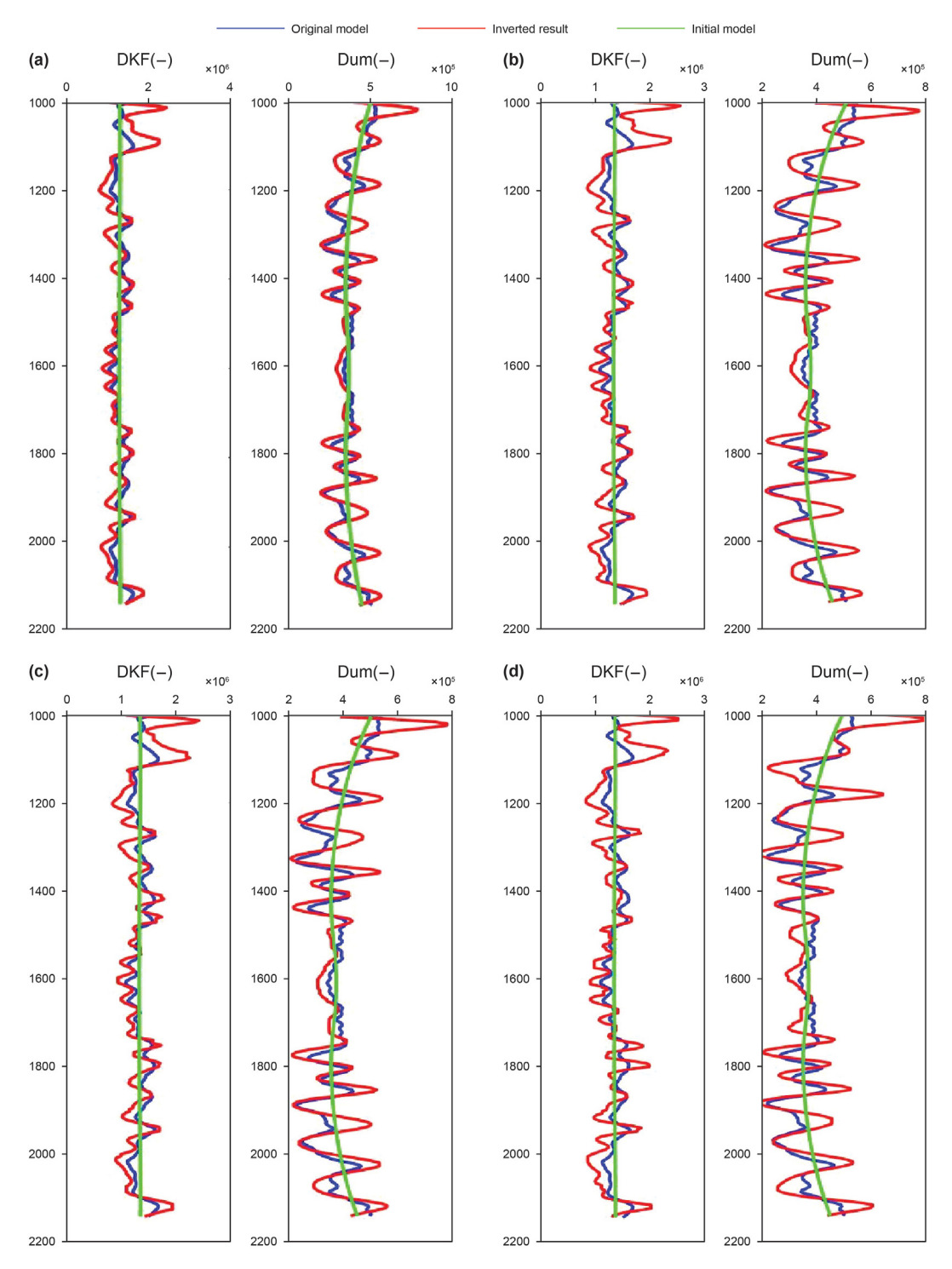


Fig. 6. Model parameter estimations $K_{f_{ane}}$ and μ_m (red means inversion result, blue means original model, green means initial model). (a). without noise; (b). S/N = 10; (c). S/N = 5; (d). S/N = 2.

from the work area. $f_0=25$ Hz is selected as the optimal reference frequency, and the multi-scale decomposition of seismic data is realized by CWT. The estimated frequency-dependent solid-liquid decoupling fluid factor profile is displayed in Fig. 8. The red block indicates the position where the hydrocarbon reservoir exists. According to logging data and inversion results, the frequency-dependent solid-liquid decoupling fluid factor shows lower anomaly in the reservoir development site, and the frequency-

dependent solid-liquid decoupling fluid factor maintains higher consistency with logging results.

4. Discussion

The conventional frequency-dependent inversion method is based on elastic medium and does not consider the seismic attenuation caused by viscoelasticity. In order to simulate the propagation Z.-Y. Zong, Y.-W. Feng, X.-Y. Yin et al. Petroleum Science 18 (2021) 1047–1058

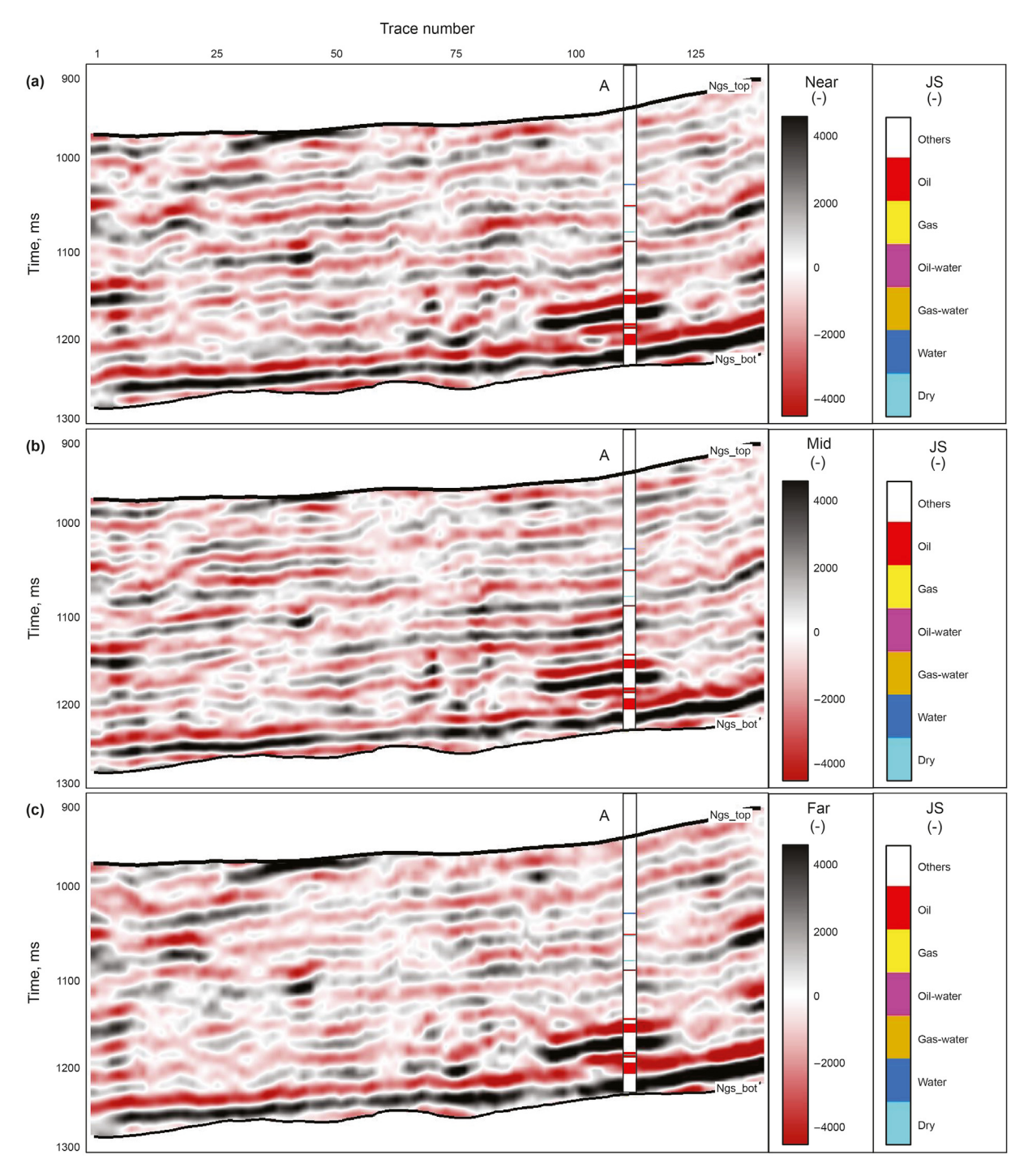


Fig. 7. Partial stacking seismic data profiles. (a). near angle stacking seismic data profile; (b). mid angle stacking seismic data profile; (c). far angle stacking seismic data

process of seismic waves in underground media, a frequency-dependent viscoelastic fluid sensitivity parameter is established based on the viscoelasticity of the media. The proposed frequency-dependent solid-liquid decoupling fluid factor by eliminating the influence of the solid rock skeleton helps to reduce the multiplicity of fluid detection to some extent, and eliminating the recognition illusion appearing during fluid detection. However, it is established incorporating the Gassmann equation and the Futterman approximation constant Q attenuation model. Further study relevant to frequency dependent viscoelastic rock physic models beyond Gassmann may be more helpful in fluid factor establishment.

By comparing with the conventional seismic reflection characteristic equation and combining with the rock physics theory, the frequency information of seismic data is deeply mined, and a new frequency-dependent viscoelastic seismic reflection characteristic equation is constructed, and its accuracy is verified. In order to simplify the derivation of the reflection coefficient equation, Taylor's first-order expansion is carried out for the convenience of inversion. It is emphasized here that the reflection coefficient characteristic equation of this paper can only carry out the first-order Taylor expansion at the reference frequency.

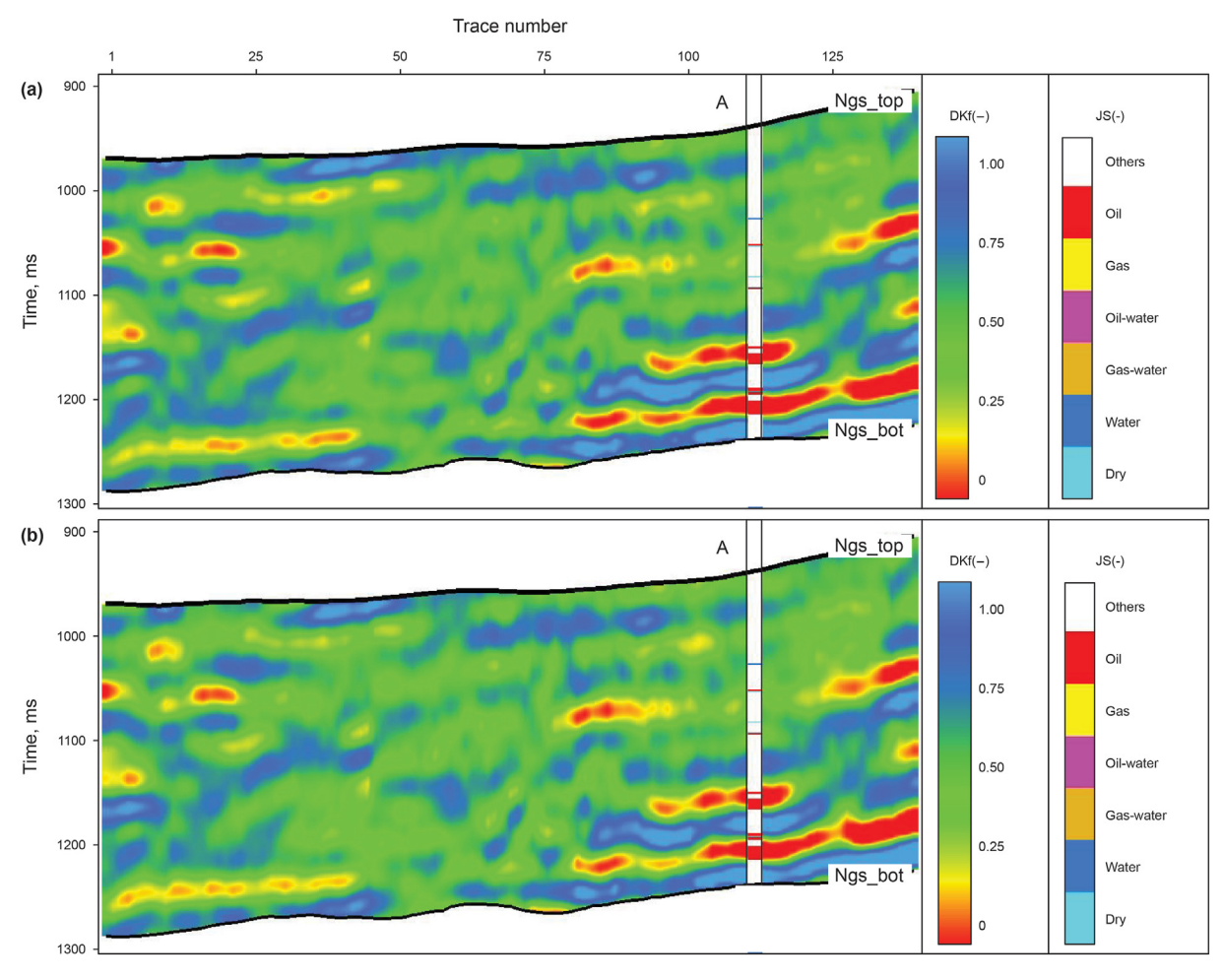


Fig. 8. Inversion result profiles. (a) frequency-dependent viscoelastic solid-liquid decoupling fluid factor profile; (b) $D\mu_{\rm m}$ profile.

5. Conclusions

A viscoelasticity and frequency-dependent amplitude variation with offsets inversion is proposed to study the underground lithology and oil/gas distribution law. Considering the viscoelasticity of the medium, a frequency-dependent solid-liquid decoupling fluid factor is constructed and the reflection characteristic equation is derived. And the frequency division of seismic data is carried out, which provides the data basis for inversion method. Under the framework of Bayesian theory, the maximum posterior probability solution is solved, and the fluid factor is finally extracted. Synthetic and field data examples demonstrate the potential of the proposed approach in fluid discrimination.

Acknowledgements

We would like to acknowledge the sponsorship of National Natural Science Foundation of China (41974119, U1762103), Science Foundation from Innovation and Technology Support Program for Young Scientists in Colleges of Shandong province and Ministry of Science and Technology of China (2020RA2C620131).

References

Ahmed, F.Y., 2012. Gas detection using matching pursuit spectral decomposition seismic attribute. EAGE Tech Program Expand Abstr. https://doi.org/10.3997/ 2214-4609.20148530.

Backus, M.M., Chen, R., 1975. Flat spot exploration. Geophys. Prospect. 23 (3),

533-577. https://doi.org/10.1111/j.1365-2478.1975.tb01547.x.

Bortfeld, R., 1961. Approximations to the reflection and transmission coefficients of plane longitudinal and transverse waves. Geophys. Prospect. 9 (4), 485–502. https://doi.org/10.1111/j.1365-2478.1961.tb01670.x.

Chapman, M., Zatsepin, S.V., Crampin, S., 2002. Derivation of a microstructural poroelastic model. Geophys J. Int 151 (2), 427–451. https://doi.org/10.1046/j.1365-246X.2002.01769.x.

Chen, G.L., Matteucci, G., Fahmy, B., et al., 2008. Spectral-decomposition response to reservoir fluids from a deepwater West Africa reservoir. Geophysics 73 (6), C23–C30. https://doi.org/10.1190/1.2978337.

Chen, H., Innanen, K.A., Chen, T., 2018. Estimating P- and S-wave inverse quality factors from observed seismic data using an attenuative elastic impedance. Geophysics 83 (2), R173–R187. https://doi.org/10.1190/geo2017-0183.1.

Chen, S.Q., Li, X.Y., Wang, S.X., 2012. The analysis of frequency-dependent characteristics for fluid detection: a physical model experiment. Appl. Geophys. 9 (2), 195–206. https://doi.org/10.1007/s11770-012-0330-8.

Cheng, G.S., Yin, X.Y., Zong, Z.Y., 2018. Third-order AVO inversion for lamé parameter based on inverse operator estimation algorithm. J. Petrol. Sci. Eng. 164, 117–126. https://doi.org/10.1016/j.petrol.2018.01.044.

Connolly, P., 1999. Elastic impedance. Lead. Edge 18 (4), 438–452. https://doi.org/ 10.1190/1.1438307.

Dai, R., Yin, C., Yang, S., et al., 2018. Seismic deconvolution and inversion with erratic data. Geophys. Prospect. 66 (9), 1684–1701. https://doi.org/10.1111/1365-2478.12689.

Downton, J.E., Lines, L.R., 2001. Constrained three parameter AVO inversion and uncertainty analysis. SEG Tech. Progr. Expand. Abstr. https://doi.org/10.1190/ 1.1816583.

Downton, J.E., 2005. Seismic Parameter Estimation from AVO Inversion. University of Calgary, Calgary, AB. https://doi.org/10.11575/PRISM/15244.

Du, Z.Y., Wu, G.C., Zong, Z.Z., 2015. Estimation method of viscoelastic fluid factor. SEG Tech. Progr. Expand. Abstr. https://doi.org/10.1190/segam2015-5895680.1.

Fatti, J.L., Smith, G.C., Vail, P.J., et al., 1994. Detection of gas in sandstone reservoirs using AVO analysis: a 3-D seismic case history using the Geostack technique. Geophysics 59 (9), 1362–1376. https://doi.org/10.1190/1.1443695.

Goodway, B., Chen, T.W., Downton, J., 1997. Improved AVO fluid detection and

- lithology discrimination using Lamé petrophysical parameters; " $\lambda \rho$ ", " $\mu \rho$ ", & " $\lambda \mu$ fluid stack", from P and S inversions. SEG Tech. Progr. Expand. Abstr. https://doi.org/10.1190/1.1885795
- Gray, D., 1999. Elastic inversion for Lamé parameters. SEG Tech. Progr. Expand. Abstr. https://doi.org/10.1190/1.1817128.
- Gray, D., Goodway, B., Chen, T.W., 1999. Bridging the gap: using AVO to detect changes in fundamental elastic constants. SEG Tech. Progr. Expand. Abstr. https://doi.org/10.1190/1.1821163.
- Han, D.H., Batzle, M.L., 2004. Gassmann's equation and fluid-saturation effects on seismic velocities. Geophysics 69 (2), 398–405. https://doi.org/10.1190/11707059
- Hedlin, K., 2000. Pore space modulus and extraction using AVO. SEG Tech. Progr. Expand. Abstr. https://doi.org/10.1190/1.1815749.
- Hilterman, F., 1990. Is AVO the seismic signature of lithology? A case history of Ship Shoal-South Addition. Lead. Edge 9 (6), 15–22. https://doi.org/10.1190/11439744
- Koefoed, O., 1955. On the effect of Poisson's ratios of rock strata on the reflection coefficients of plane waves. Geophys. Prospect. 3 (4), 381–387. https://doi.org/ 10.1111/i.1365-2478.1955.tb01383.x.
- Li, G.F., Zhang, H.L., Wang, Y.J., et al., 2014. Prestack AVO inversion using edgepreserving regularization with directional constraints. SEG Tech. Progr. Expand. Abstr. https://doi.org/10.1190/segam2014-0091.1.
- Li, K., Yin, X.Y., Zong, Z.Y., 2017. Bayesian seismic multi-scale inversion in complex Laplace mixed domains. Petrol. Sci. 14 (4), 694–710. https://doi.org/10.1007/s12182-017-0191-0
- Li, K., Yin, X.Y., Zong, Z.Y., 2016. Time frequency domain FAVO fluid discrimination method based on matching pursuit spectrum decomposition. Acta Pet. Sin. 37 (6), 777–786.
- Li, K., Yin, X.Y., Zong, Z.Y., et al., 2020. Seismic AVO statistical inversion incorporating poroelasticity. Petrol. Sci. 17 (5), 1237–1258. https://doi.org/10.1007/s12182-020-00483-5.
- Liu, Z., Wang, Y., 2013. A joint high-resolution processing method and its application for thin inter-beds. Petrol. Sci. 10 (2), 195–204. https://doi.org/10.1007/s12182-013-0267-4.
- Mazzotti, A., 1991. Amplitude, phase and frequency versus offset applications. Geophys. Prospect. 39 (7), 863–886. https://doi.org/10.1111/j.1365-2478.1991.tb00348.x.
- Murphy, W., Reischer, A., Hsu, K., 1993. Modulus decomposition of compressional and shear velocities in sand bodies. Geophysics 58 (2), 227–239. https://doi.org/10.1190/1.1443408.
- Muskat, M., Meres, M.W., 1940. Reflection and transmission coefficients for plane waves in elastic media. Geophysics 5 (2), 115–148. https://doi.org/10.1190/11441797
- Ostrander, W.J., 1984. Plane-wave reflection coefficients for gas sands at nonnormal angles of incidence. Geophysics 49 (10), 1637–1648. https://doi.org/10.1071/FC984193a
- Pan, X.P., Zhang, G.Z., Zhang, J.J., et al., 2017. Zoeppritz-based AVO inversion using an improved Markov chain Monte Carlo method. Petrol. Sci. 14 (1), 75–83. https:// doi.org/10.1007/s12182-016-0131-4.
- Quakenbush, M., Shang, B., Tuttle, C., 2006. Poisson impedance. Lead. Edge 25 (2), 128–138. https://doi.org/10.1190/1.2172301.
- Ren, H.T., Goloshubin, G., Hilterman, F.J., 2009. Poroelastic analysis of amplitude-versus-frequency variations. Geophysics 74 (6), N41–N48. https://doi.org/10.1190/1.3207863.
- Richards, P.G., Aki, K., 1980. Quantitative Seismology: Theory and Methods. W. H. Freeman and Co., London.
- Russell, B.H., Gray, D., Hampson, D.P., 2011. Linearized AVO and poroelasticity.

- Geophysics 76 (3), C19-C29. https://doi.org/10.1190/1.3555082.
- Shuey, R.T., 1985. A simplification of the Zoeppritz equations. Geophysics 50 (4), 609–614. https://doi.org/10.1190/1.1441936.
- Smith, G.C., Gidlow, P.M., 2003. The fluid factor angle and the crossplot angle. SEG Tech. Progr. Expand. Abstr. https://doi.org/10.1190/1.1817679.
- Smith, G.C., Gidlow, P.M., 1987. Weighted stacking for rock property estimation and detection of gas. Geophys. Prospect. 35 (9), 993–1014. https://doi.org/10.1111/ j.1365-2478.1987.tb00856.x.
- Tatham, R.H., 1982. Vp/Vs and lithology. Geophysics 47 (3), 336–344. https://doi.org/10.1190/1.1441339.
- Wang, Y.H., 1999. Approximations to the Zoeppritz equations and their use in AVO analysis. Geophysics 64 (6), 1920–1927. https://doi.org/10.1190/1.1444698.
- Weilian, L., 2007. Determination of lateral extension of hydrocarbon concentration sealing caprocks by AVO analysis. Petrol. Sci. 4, 17–22. https://doi.org/10.1007/BF03187451
- Whitcombe, D.N., 2002. Elastic impedance normalization. Geophysics 67 (1), 60–62. https://doi.org/10.1190/1.1451331.
- Wilson, A., Chapman, M., Li, X.Y., 2009. Frequency-dependent AVO inversion. SEG Tech. Progr. Expand. Abstr. https://doi.org/10.1190/1.3255572.
- Wu, X.Y., Chapman, M., Wilson, A., et al., 2010a. Estimating seismic dispersion from pre-stack data using frequency-dependent AVO inversion. SEG Tech. Progr. Expand. Abstr. https://doi.org/10.1190/1.3513759.
- Wu, X.Y., Chapman, M., Wilson, A., et al., 2010b. Frequency dependent AVO inversion using smoothed pseudo Wigner-Ville distribution. In: 72nd EAGE Conference & Exhibition incorporating SPE EUROPEC.
 Yao, G., Wu, D., 2017. Reflection full waveform inversion. Sci. China Earth Sci. 60
- Yao, G., Wu, D., 2017. Reflection full waveform inversion. Sci. China Earth Sci. 60 (10), 1783–1794. https://doi.org/10.1007/s11430-016-9091-9.
- Yao, G., Wu, D., Wang, S.X., 2020. A review on reflection-waveform inversion. Petrol. Sci. 17 (2), 334–351. https://doi.org/10.1007/s12182-020-00431-3. Yin, X.Y., Zhang, S.X., Zhang, F.C., et al., 2010. Utilizing Russell approximation-based
- Yin, X.Y., Zhang, S.X., Zhang, F.C., et al., 2010. Utilizing Russell approximation-based elastic wave impedance inversion to conduct reservoir description and fluid identification. OGP 45 (3), 373–380. https://doi.org/10.1016/S1872-5813(11) 60005-4 (in Chinese).
- Yin, X.Y., Zong, Z.Y., Wu, G.C., 2013. Improving seismic interpretation: a high-contrast approximation to the reflection coefficient of a plane longitudinal wave. Petrol. Sci. 10 (4), 466–476. https://doi.org/10.1007/s12182-013-0297-y.
- Zhang, F.C., Dai, R.H., Liu, H.Q., et al., 2014. Multi-frequency AVA simultaneous inversion for prestack seismic gathers. SEG Tech. Progr. Expand. Abstr. https:// doi.org/10.1190/segam2014-0719.1.
- Zhang, R., Sen, M.K., Srinivasan, S., 2012. A prestack basis pursuit seismic inversion. Geophysics 78 (1), R1–R11. https://doi.org/10.1190/geo2011-0502.1.
- Zhang, S.X., Yin, X.Y., Zhang, G.Z., 2011. Dispersion-dependent attribute and application in hydrocarbon detection. J. Geophys. Eng. 8 (4), 498–507. https://doi.org/10.1088/1742-2132/8/4/002.
- Zhang, Y.Y., Jin, Z.J., Chen, Y.Q., et al., 2018. Pre-stack seismic density inversion in marine shale reservoirs in the southern Jiaoshiba area, Sichuan Basin, China. Petrol. Sci. 15, 484–497. https://doi.org/10.1007/s12182-018-0242-1.
- Zhu, X.F., McMechan, G.A., 2012. Elastic inversion of near-and postcritical reflections using phase variation with angle. Geophysics 77 (4), R149–R159. https:// doi.org/10.1190/geo2011-0230.1.
- Zoeppritz, K.B., 1919. Über Reflexion ad Durchgang seismischer wellen durch Unstetigkeitsflachen: Göttinger Nach Mathematisch-physikalische Klasse. Erdbebenwellen VIII B K1, 66–84.
- Zong, Z.Y., Yin, X.Y., Wu, G.C., 2012. AVO inversion and poroelasticity with P-and S-wave moduli. Geophysics 77 (6), N17–N24. https://doi.org/10.1190/geo2011-0214.1.